Magnetic Logic Gate Based on Polarized Spin Waves

Weichao Yu (余伟超),[1,†] Jin Lan (兰金),[1,2] and Jiang Xiao (萧江)[1,3,*]

[1] *Department of Physics and State Key Laboratory of Surface Physics, Fudan University, Shanghai 200433, China*

[2] *Center of Joint Quantum Studies and Department of Physics, School of Science, Tianjin University, Tianjin 300350, China*

[3] *Institute for Nanoelectronics Devices and Quantum Computing, Fudan University, Shanghai 200433, China*

(Received 17 June 2019; revised manuscript received 5 December 2019; accepted 10 January 2020; published 21 February 2020)

Spin wave, the precession of magnetic order in magnetic materials, is a collective excitation that carries spin angular momentum. Similar to acoustic or optical waves, the spin wave also possesses the polarization degrees of freedom. Although such polarization degrees of freedom are frozen in ferromagnets, they are fully unlocked in antiferromagnets or ferrimagnets. Here we introduce the concept of magnetic gating and demonstrate a spin-wave analog of the Datta-Das spin transistor in antiferromagnets. Utilizing the interplay between polarized spin wave and the antiferromagnetic domain walls, we propose a universal logic gate of pure magnetic nature, which realizes all Boolean operations in one single magnetic structure.

DOI: 10.1103/PhysRevApplied.13.024055

I. INTRODUCTION

How to go beyond "Moore's law" is of great interest for both fundamental scientific researches and industrial enterprises [1,2]. The core issue of the present silicon technology is the enormous energy dissipation caused by the shrinking dimensions of transistors and the von-Neumann architecture [3]. Developing the non-von-Neumann architecture, or more specifically the in-memory computing architecture, is a promising route towards easing the issues faced in the information technologies.

At present, most of the developments in spintronics, including the discovery of giant magnetoresistance (GMR) [4,5], spin-transfer torque (STT) [6,7], spin-orbit torque (SOT) [8], and the invention of the STT and SOT MRAM and the magnetic racetrack memories [9,10], concentrate on data storage. And they all rely on the spin current carried by the conduction electrons, which gives rise to the unavoidable Joule heating. To go beyond above limitations of spintronics, it is highly desirable to employ the types of spin carriers that not only dissipate less but can serve both purposes of data storage and processing. One of the promising candidates is the spin wave (or magnon) [11,12], the collective precession of ordered magnetization in magnetic materials. The mutual control between spin waves and magnetic domain walls was recently demonstrated experimentally for the first time by Han *et al.* [13], which strengthens the applicability of the computing scheme proposed in this paper.

For the purpose of data processing based on spin waves, most efforts so far have used the spin-wave amplitude or phase to encode information [14–18,18–21]. However, it is more natural to use the more robust polarization degree of freedom to encode information [22]. In ferromagnets, the polarization freedom is frozen because only the right-circular polarization is allowed. In antiferromagnets, there are two degenerate eigenmodes precessing in opposite directions, i.e., the left- and right-circular polarization [22–25], which are sometimes referred to as the spin-wave chirality [26], helicity [27], or isospin [28]. With two circular modes, spin waves possessing arbitrary polarizations can be constructed, just like its optical counterparts.

In this paper, we introduce the concept of magnetic gating, where the exchange field from a magnetic gating layer can shift the spin-wave dispersions in an antiferromagnet. In the meantime, the degeneracy of the two circular spin-wave modes is lifted by the gating magnetization, causing a polarization rotation for the linearly polarized spin waves. This magnetic gating effect on spin-wave polarizations, together with the polarization-selective spin-wave-driven domain-wall motion presented by the same authors previously [29], forms a complete interconversion scheme between the static magnetic texture and dynamical spin waves via the polarization channel. Based on this scheme, we propose a purely magnetic logic gate, whose inputs and outputs are both the nonvolatile magnetic racetrack memories [9,10], and the information processing in between is accomplished by polarized spin waves. Because of the interaction between the polarized spin wave and

*xiaojiang@fudan.edu.cn

†Present address: Institute for Materials Research, Tohoku University, Sendai, Japan.

antiferromagnetic domain wall possesses a special feature of double threshold behavior, such a magnetic logic gate is capable of achieving all unary and binary logic operations in one single hardware structure.

II. MODEL

For simplicity, instead of a real antiferromagnet, we consider a synthetic antiferromagnet (SyAF) consisting of two spatially separated magnetic sublayers extending in x direction [30,31], as depicted in the insets of Fig. 1(a).

The two sublayers are coupled antiferromagnetically via the Rudderman-Kittel-Kasuya-Yosida (RKKY) interaction across a metallic spacer layer [32]. The magnetization dynamics of the SyAF is described by the coupled Landau-Lifshitz-Gilbert (LLG) equations [22,24]

$$\dot{\mathbf{m}}_j(x,t) = -\gamma \mathbf{m}_j(x,t) \times \mathbf{H}_j^{\text{eff}} + \alpha \mathbf{m}_j(x,t) \times \dot{\mathbf{m}}_j(x,t), \tag{1}$$

where $j = 1, 2$ denotes the lower and upper sublayer, respectively, γ is the gyromagnetic ratio, and α is the Gilbert damping constant. Here $\mathbf{H}_j^{\text{eff}} = Km_j^z\hat{\mathbf{z}} + A\nabla^2\mathbf{m}_j - J\mathbf{m}_{\bar{j}} + \mathbf{H}_j$ (with $\bar{1} = 2, \bar{2} = 1$) is the effective magnetic field acting on sublayer $\mathbf{m}_j$, where K is the easy-axis anisotropy along $\hat{\mathbf{z}}$, A and J are the intra and interlayer exchange coupling coefficients, and $\mathbf{H}_j$ is the external magnetic field.

The equilibrium magnetization of the two sublayers $\mathbf{m}_{1,2}^0$ points in $\mp\hat{\mathbf{z}}$ direction, respectively. Upon this collinear magnetic configuration, we separate the static and dynamical components of the sublayer magnetization as $\mathbf{m}_j(x,t) = \mathbf{m}_j^0 + \delta\mathbf{m}_j(x,t)$, where $\delta\mathbf{m}_j = m_j^x\hat{\mathbf{x}} + m_j^y\hat{\mathbf{y}}$ is the transverse dynamical component of spin wave. By linearizing the LLG equation Eq. (1) to the leading order of $\tilde{m}_j \equiv m_j^x - im_j^y$, and ignoring the damping term, the spin-wave dynamics reduces to

$$(-1)^j i\frac{\partial}{\partial t}\tilde{m}_j = \gamma\left[-A\nabla^2 + K + J + (-1)^j H_j\right]\tilde{m}_j + \gamma J\tilde{m}_{\bar{j}}. \tag{2}$$

When the external field vanishes ($H_j = 0$), Eq. (2) hosts two degenerated circularly polarized spin-wave modes with dispersions as $\omega_{L/R}(k) = \gamma\sqrt{(Ak^2 + K + J)^2 - J^2}$ for the left- and right-circular mode, where k is the wavevector along $\hat{\mathbf{x}}$.

III. SPIN-WAVE POLARIZATION MANIPULATION VIA MAGNETIC GATING

To lift the degeneracy between these two circular spin-wave modes, we introduce a modified SyAF structure by capping a magnetic gating layer ($\mathbf{m}_G$) upon the SyAF [see Fig. 1(a)]. The gating layer is antiferromagnetically coupled to the upper layer of SyAF via RKKY with strength $2J'$. For simplicity, the gating layer magnetization is pinned along the $\hat{\mathbf{z}}$ axis with $\mathbf{m}_G = \pm\hat{\mathbf{z}}$. The magnetic gating effect of $\mathbf{m}_G$ on SyAF is introduced via the exchange field $\mathbf{H}_2 = -2J'\mathbf{m}_G$ from the gating layer on the

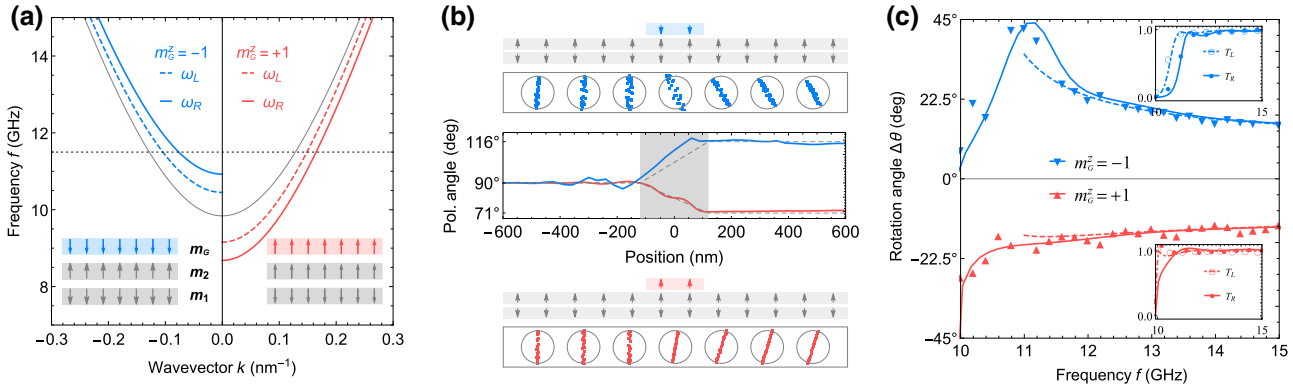

FIG. 1. Magnetic gating effect on spin-wave polarization. (a) Spin-wave dispersions for the left- and right-circular modes for ungated (gray), up-gated (red), and down-gated (blue) SyAF. Inset: a SyAF gated magnetically by the capping layer $\mathbf{m}_G$. (b) Spatial variation of the spin-wave polarization across an ungated-gated-ungated SyAF junction extracted from the micromagnetic simulations. The vertically polarized spin wave of frequency $f = 11.5$ GHz is injected from the left side. Top and bottom: the Lissajous-like pattern showing the stagger order $n^{x,y} \equiv (m_2^{x,y} - m_1^{x,y})/2$ for the down and up-gated case. Data for about eight periods (in total 0.625 ns) are included for each circle. The total number of pixels in each circle is 34, and each pixel corresponds to the stagger order for a specific time. The time separation between two pixels is about 0.02 ns, corresponding to six minimal time steps (about 0.003 ns). Middle: the polarization angle as a function of position. (c) Spin-wave polarization rotation angle $\Delta\theta$ as a function of spin-wave frequency for a down and up-gated SyAF. Data points are extracted from micromagnetic simulations, and the curves are calculated from a full scattering calculation (solid) and the WKB approximation (dashed). Insets: the transmission probability across the magnetic-gating region. All figures in the paper use the following parameters: $\gamma = 2.21 \times 10^5$ A/m, $K = 3.88 \times 10^4$ A/m, $A = 0.328 \times 10^{-11}$ A m, $J = 10^6$ A/m, and $J' = 0.675 \times 10^4$ A/m. For (b),(c), the length of the gating region is $l = 240$ nm.

upper sublayer, while the lower sublayer is not affected (thus $\mathbf{H}_1 = 0$). This magnetic gating field modifies the spin-wave dispersions in the SyAF [22,33] to

$$\omega_{L/R}(k) = \gamma\sqrt{(Ak^2 + K + J - J'm_G^z)^2 - J^2} \mp \gamma J' m_G^z, \tag{3}$$

where $m_G^z = \pm 1$ denotes the magnetization direction of the gating layer [34].

The modified dispersions in Eq. (3) are plotted in Fig. 1(a), showing that the magnetic gating either increases or decreases the spin-wave gap depending on the gating magnetization direction ($\mathbf{m}_G = \pm\hat{z}$). In the meantime, the magnetic gating lifts the degeneracy between the left- and right-circular modes due to the preferential coupling between the capping layer and the upper sublayer of SyAF. Consequently, the left- and right-circular modes with the same frequency ω would propagate at different wavevectors $k_{L,R}$ with $\omega = \omega_L(k_L) = \omega_R(k_R)$, which results in a relative phase delay between the right- and left-circular spin-wave components. The magnetic gating effect here is realized via RKKY interaction between the capping ferromagnet and SyAF. Similar gating effect should be possible via the exchange bias effect between ferromagnet and real antiferromagnet [35], for controlling the spin-wave polarizations in the latter.

When a linearly polarized spin wave of frequency ω is passing through a gating segment of length l, this relative phase delay induces a rotation of the linear polarization by angle $\Delta\theta = (k_L - k_R)l/2$, where $k_{L/R}$ satisfies Eq. (3) with $\omega_{L/R}(k_{L/R}) = \omega$. In WKB approximation, the magnetization-dependent rotation angle

$$\Delta\theta \approx -\frac{\omega}{\sqrt{\omega^2 + \gamma^2 J^2}}\eta(1-\eta)k_0 l, \tag{4}$$

where $\eta = (J'/2Ak_0^2)m_G^z$ denotes the gating efficiency, and k_0 is the wavevector without gating. As seen, the rotation direction is explicitly controlled by the gating magnetization direction m_G^z via η. The different rotation angle for the up and down-gated case is due to the quadratic spin-wave dispersions in Eq. (3). In addition, for the down-gated case ($m_G^z = -1$) as shown in Fig. 1(a), the increased spin-wave gap effectively introduces a potential barrier in the gated region, which causes a slight reflection. It is this small amount of reflection that induces some nonregularity of the Lissajous-like pattern in the upper panels of Fig. 1(b). For the up-gated case ($m_G^z = +1$), the lowering dispersions of the gated region is effectively a potential well, which has much less reflection, and the resulting polarization is much cleaner as seen in the lower panels of Fig. 1(b).

This magnetic-gating-induced polarization rotation is a spin-wave analog of the Datta-Das spin transistor [36]: the spin-wave polarization rotates in opposite directions when the magnetic gating reverses or m_G^z changes sign. This spin-wave Datta-Das field transistor is of purely magnetic nature, and thus is different from the spin-wave field transistor proposed by Cheng *et al.* using an electrical gating of the Dzyaloshinnski-Moriya interaction (DMI) [24]. Figure 1(b) shows a micromagnetic simulation of the magnetic gating effect on a linear y (90°) polarized spin wave of frequency $f = \omega/2\pi = 11.5$ GHz. It is seen that, as the spin wave passes across the magnetic gating region, its linear polarization steadily rotates (counter)clockwise, and finally acquires a rotation angle of $\Delta\theta = +26°/-19°$ for down and upgating according to Eq. (4). The frequency dependence of the rotation angle $\Delta\theta$ is shown in Fig. 1(c), agreeing with the scattering calculations and the WKB expression in Eq. (4). The dipolar field only leads to a simple reduction of the interlayer coupling J' in the spin-wave rotation, and thus is neglected here.

The magnetic gating provides the capability of converting the information from static magnetic domains to polarized spin waves. To form a complete interchanging scheme between static magnetic domains and dynamical spin waves, one needs an extra ingredient of manipulating magnetic domains via polarized spin wave. It is known that, in the presence of DMI (which naturally exists in SyAF), the antiferromagnetic domain wall reflects spin waves differently according to its linear polarization [22]. As shown in Refs. [22] and [29], the dynamics of the spin-wave scattering by an antiferromagnetic domain wall can be described by a set of Klein-Gordon-like equations

$$\gamma\partial_t^2 n_x = J[A\partial_x^2 - U_K(x)]n_x, \tag{5a}$$

$$\gamma\partial_t^2 n_y = J[A\partial_x^2 - U_K(x) - U_D(x)]n_y, \tag{5b}$$

where $\partial_t \equiv \partial/\partial t$, $\partial_x \equiv \partial/\partial_x$, and $n_{x,y} \equiv m_1^{x,y} - m_2^{x,y}$ is the x/y component of the staggered magnetization. Here $U_K(x) = K[1 - 2\mathrm{sech}^2(x/W)]$ is the effective (reflectionless) potentials arising from the easy-axis anisotropy at the domain wall of width W. And the DMI-induced effective potential $U_D(x) = (D/W)\mathrm{sech}(x/W)$ acts as an effective hard axis for the y component, which causes reflections for y-polarized spin wave only. Because of the component-dependent effective potentials, the spin-wave reflectivity strongly depends on its polarization: $R_x \approx 0$ while $R_y > 0$. The reflected spin wave transfers linear momentum to the domain wall, pushing the domain wall forward. Assumed as a rigid object, the domain wall is parameterized by its location X, which satisfies a Newtonian-type equation of motion [29]:

$$\frac{1}{WJ}\frac{\partial^2 X}{\partial t^2} + \frac{4\alpha}{W}\frac{\partial X}{\partial t} = \rho^2 Ak^2 R_{x,y}, \tag{6}$$

where ρ is the incoming spin-wave amplitude. Equation (6) indicates that the domain wall is pushed forward by

the reflected polarization ($\hat{\mathbf{y}}$ polarization here, $R_y > 0$) but stays still for the transmitting polarization ($\hat{\mathbf{x}}$ polarization, $R_x \approx 0$) [29].

IV. SPIN-WAVE-BASED LOGIC GATES

With the two complementary ingredients, i.e., the magnetic gating effect in manipulating spin-wave polarization and the polarization-dependent domain-wall motion, we are ready to construct logic gates of purely magnetic nature.

A. Unary gates

The simplest logic gate of all is the NOT gate. A magnetic NOT gate, shown in Fig. 2(a), consists of two magnetic racetrack memories bridged by a logic track made of SyAF. All adjacent layers are coupled antiferromagnetically via RKKY interaction. The input and output bits are stored as magnetic domains in the racetrack memory with spin up and down for bit 1/0. In the logic track, an antiferromagnetic domain wall is located close to the output track. The linearly polarized spin wave is injected from the left and propagates along the logic track toward the domain wall. Without driving spin waves, the domain wall stays at or relaxes back to position P_1, by anisotropy gradient for example [37]. Under influence of driving spin waves, the domain wall may or may not be pushed up to position P_2, depending on the polarization of the incoming spin wave. In the simulation, the amplitude of the driving spin wave corresponds to a cone angle of approximately 5.7°, which is comparable to spin-wave strength (approximately 5°) realized in the recent experiment demonstrating the spin-wave-driven domain-wall motion [13].

The magnetization in the input memory track acts as a magnetic gate, modulating the spin-wave polarization running in the logic track according to the input bit: the bit 0 (1) corresponds to up(down)-gating. For a NOT gate, the polarization of injected spin waves (of frequency f = 11 GHz) is chosen as $\theta_i = 106°$, and the length of the gating region (equal to the width of the input track) is $l = 240$ nm such that an overall rotation angle of $\Delta\theta_0 = +29°$ for bit 0 or $\Delta\theta_1 = -16°$ for bit 1, and $\Delta\theta_0 - \Delta\theta_1 = 45°$ [38]. Via the magnetic gating, the bit information stored in the input track is read out and encoded into the rotated spin-wave polarization in the logic track: $\theta_{0/1} = \theta_i + \Delta\theta_{0/1} = 135°/90°$ for bit 0/1, as shown in the polarization rotation diagram for NOT in Fig. 2.

The following information processing is realized using the polarization-selective spin-wave-driven domain-wall motion mentioned above and detailed in Ref. [29]. More specifically for the NOT gate, the modulated spin wave, after being gated by the input bit 1, is polarized along $\hat{\mathbf{y}}$ (90°), therefore the spin wave is completely reflected and this transfers enough momentum to push the domain-wall position P_1 across the output track to position P_2. On the other hand, the modulated spin wave gated by input bit 0 has 135° polarization, far away from $\hat{\mathbf{y}}$ polarization, the reflection is small, and the domain wall stays at or returns to P_1.

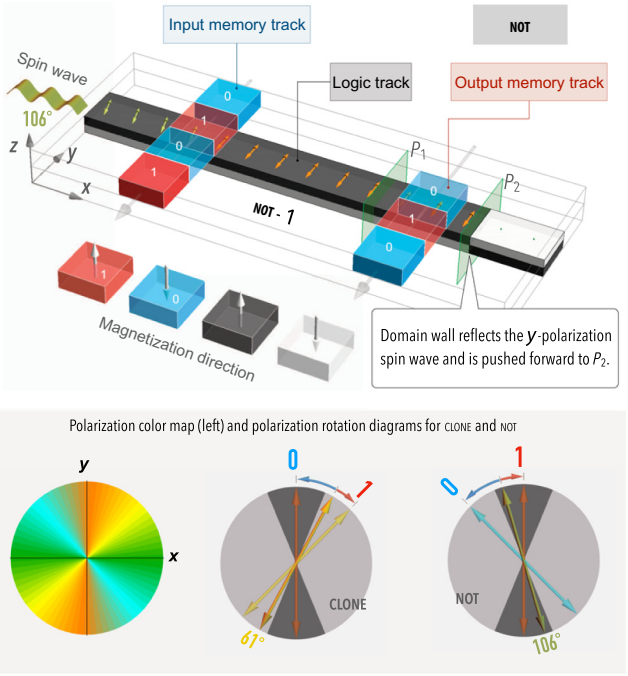

FIG. 2. A magnetic unary gate consists of an input and an output memory track (magnetic racetrack memory) bridged by a logic track (a SyAF wire with a domain wall). The racetrack memories can be driven by electric current to shift the desired bit into (out of) the logic track. This unary gate realizes the NOT function for $\theta_i = 106°$ (as shown), but the CLONE function for $\theta_i = 61°$ (not shown). Bottom: the color map of the linear spin-wave polarization (left), the polarization rotation diagram for the CLONE gate (middle) and the NOT gate (right). The shaded area indicates the polarization angles, which can push the domain wall to P_2.

The output is written to the output memory via magnetic imprinting: because the magnetizations in the upper sublayer of SyAF and the output track are always opposite, when the domain wall is at P_1, the upper sublayer magnetization of SyAF is up, and thus the magnetization in the output track is down, corresponding to bit 0. The overall results are for the input bit 1 (0), the modulated spin wave pushes the domain wall to P_1 (P_2), and thus bit 0 (1) is imprinted to the output track, realizing a NOT gate with $1 \rightarrow 0$ and $0 \rightarrow 1$. Multiple cycles of NOT operations are simulated using micromagnetic simulations (see Video 1).

A unique advantage of this magnetic logic is its extreme configurability. As shown above, the gate structure in Fig. 2 functions as a NOT gate when injecting spin wave with polarization $\theta_i = 106°$. Merely by changing the injection polarization to $\theta_i = 61°$, this unary gate manifests

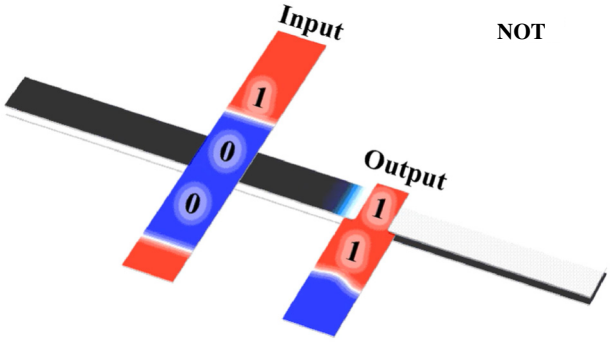

VIDEO 1. Micromagnetic simulation video showing the workflow of a 1-bit NOT gate. The injected spin waves are 106° polarized. The simulation duration is 40 ns so that there are four operation cycles demonstrated.

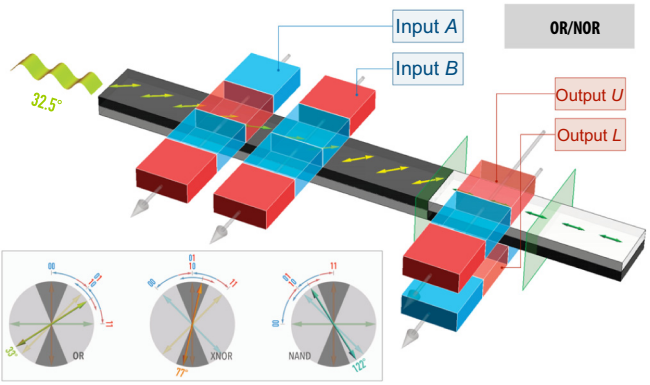

FIG. 3. A magnetic binary gate consists of two input racetrack memories and (at least) one output racetrack, bridged by a logic track. Inset: the polarization rotation diagram for the OR/XNOR/NAND gate with the initial polarization angle 32°/77°/122°.

itself as a CLONE gate, i.e., cloning the input bit to the output memory.

B. Binary gates

For the binary gates, there are three possible input combinations: 00, 01/10, 11 and two possible outputs: 0 or 1, therefore there are in total $2^3 = 8$ distinct gates. These include six nontrivial gates: OR, AND, NOR, NAND, XOR, XNOR, and two trivial gates that map all input combinations unanimously to either 0 or 1 (called ZERO and UNITY here).

The binary gates can be extended from the unary gate by adding one more input track as depicted in Fig. 3, which has now two input memory tracks (A and B) and two output tracks (U and L), bridged by an SyAF logic track. Since all adjacent layers are coupled antiferromagnetically, the upper and lower output (U and L) always yield opposite results, e.g., if output U is logic OR, then output L gives logic NOR.

With two input tracks, the injected spin wave is gated by two consecutive magnetic gating segments. Because the polarization rotation caused by bit 0 and bit 1 are the opposite, the overall rotation can be either enhanced when the inputs are the same (00 or 11), or reduced when the inputs are different (01 or 10). For three different input combinations, the spin-wave polarization would rotate by $\Delta\theta_{00} = 2\Delta\theta_0 = +58^\circ$ for input 00, $\Delta\theta_{11} = 2\Delta\theta_1 = -32^\circ$ for input 11, and $\Delta\theta_{01} = \Delta\theta_{10} = \Delta\theta_0 + \Delta\theta_1 = +13^\circ$ for input 01 or 10, each separated by exactly 45°.

When the injected spin wave has polarization angle $\theta_i = +32^\circ$ (as shown in Fig. 3), the modulated polarization after gating becomes $\theta_{00} = 90^\circ$ for input 00, $\theta_{11} = 0^\circ$ for input 11, and $\theta_{01} = \theta_{10} = 45^\circ$ for input 01 or 10, respectively. Since only θ_{00} has a large enough $\hat{\mathbf{y}}$ component (within the shaded area in the rotation diagrams in Fig. 3), the domain wall moves across the output tracks to P_2 only for input 00, and the moved domain wall imprints bit 0 to the output U track: $00 \rightarrow 0$. For all other inputs, the domain wall stays at P_1, which writes bit 1 to the output U track: $01/10/11 \rightarrow 1$. Therefore, the binary gate shown in Fig. 3, with injecting polarization $\theta_i = +32^\circ$, realizes an OR gate in the output U track, and in the meantime a NOR gate in the output L (see Video 2).

Similar to the unary gate, the binary-gate structure in Fig. 3 can also serve as multiple different gates by simply altering the polarization of the injected spin waves. Based on the polarization rotation diagrams in Fig. 3, the gates OR/XNOR/NAND (NOR/XOR/AND) are realized in the output U

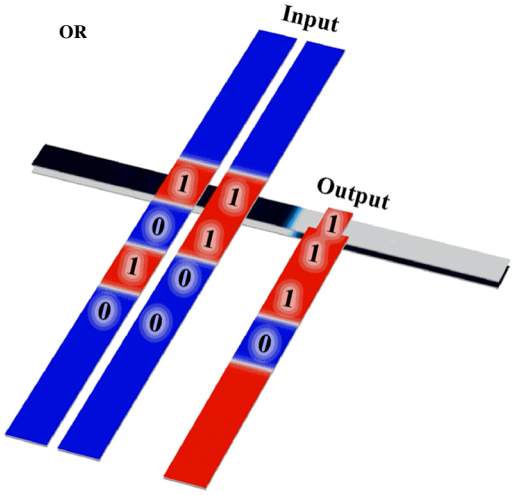

VIDEO 2. Micromagnetic simulation video showing the workflow of a 2-bit OR gate. The injected spin waves are 32.5° polarized. The simulation duration is 50 ns so that five operation cycles are demonstrated. The demonstration covers the full cycle of the 2-bit truth table and is proven to work as an OR gate as shown Fig. 3.

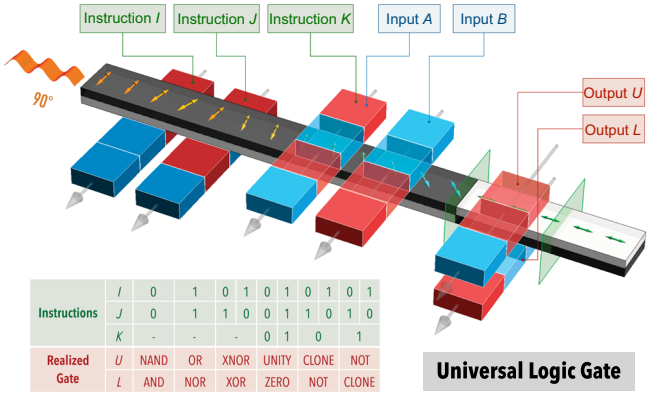

Instructions	I	0	1	0	1	0	1	0	1	0	1
	J	0	1	1	0	0	1	1	0	1	0
	K	-	-	-	-	0	1	0	1		
Realized Gate	U	NAND	OR	XNOR	UNITY	CLONE	NOT				
	L	AND	NOR	XOR	ZERO	NOT	CLONE				

FIG. 4. The universal logic gate with two instruction tracks (I, J) can realize all unary and binary logic gates with fixed 90° spin-wave polarization injection. Inset: the instruction table for realizing different gates.

(L) track when the injected spin waves are polarized along 32°/77°/122°.

C. Universal gate

Although the unary and binary gates above can realize different gate functions by varying injected spin-wave polarizations, it is inconvenient to do so. To avoid this complication, we propose a universal logic gate as shown in Fig. 4, which uses two more instruction tracks (I, J). According to the bits in the instruction tracks, the 90° polarized spin wave can be preprocessed into the desired 32°/77°/122° polarization. For instance, when the instruction bits are IJ = 10, the polarization after the instruction tracks is 77°, realizing XNOR/XOR for the output U/L. This structure can also function as a unary gate by using the input A as the third instruction K. For instance, when IJK = 010, it is a CLONE/NOT gate from input B to output U/L.

According to the instruction table in Fig. 4, this structure realizes all ten unary and binary logic gates, therefore we call it a universal logic gate. In other words, a magnetic logic gate using only one logic track can realize multiple functionalities, which usually require a dozen of conventional electronic gates. Micromagnetic simulations confirm the functioning of the universal logic gate (see Video 3).

V. DISCUSSIONS

A. Double-threshold nonlinearity

A Boolean logic maps an n-bit input to a 1-bit output. When treating the input and output bits in equal foot, there are $n+1$ possible bits, and thus in total 2^{n+1} different types of gates. Two of them are trivial gates, which unanimously map all inputs to 0 (or 1), and the rest $2^{n+1}-2$ gates are nontrivial logic gates. For example, there are two nontrivial unary gates ($n=1$): the CLONE and NOT gate, and there

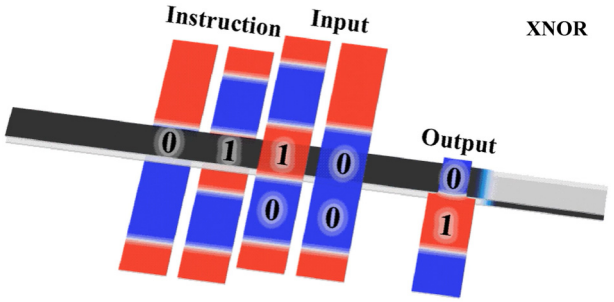

VIDEO 3. Micromagnetic simulation video showing the workflow of a universal gate. The injected spin waves are 90° polarized (linear y polarization). The Gilbert damping is reduced to 3.6×10^{-4} to compensate the additional propagation length induced by the instruction tracks. The simulation duration is 120 ns so that 12 operation cycles are demonstrated. The 12 operations cover the full cycle of the 2-bit truth table ($2^2=4$ operations) three times. According to different instructions 11/00/01, the universal gate works as OR/NAND/XNOR, respectively, which is consistent with Fig. 4.

are six nontrivial binary gates ($n=2$): the AND, OR, XOR, NAND, NOR, XNOR gate. In order to realize logic gates, physical systems with nonlinearity are required. A typical nonlinear physical behavior is the threshold behavior, i.e., some physical property undergoes an abrupt change when the input is above a certain threshold (see the top panel of Fig. 5). Typically, the strength of the input is a monotonic function of the number of 1s in the input. Therefore, the input strength increases in sequence of 00, 01/10, 11. When the threshold is set to be between 00 and 01/10, it distinguishes 00 from 01/10 and 11 and realizes an OR gate. When the threshold is between 01/10 and 11, it realizes an AND gate. However, the single threshold behavior cannot realize the XOR gate, which distinguishes input 01/10 from 00 and 11.

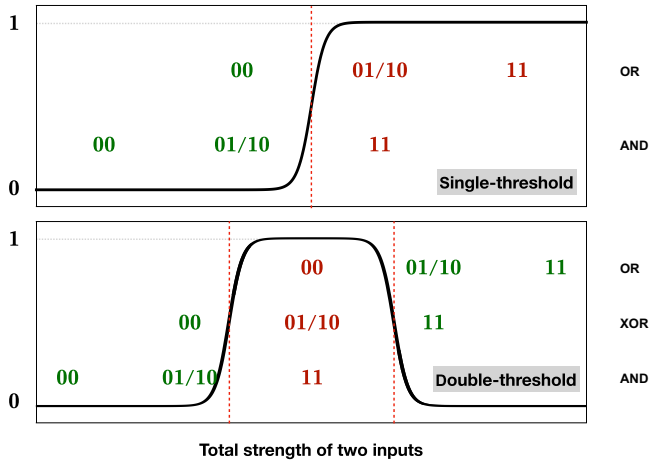

FIG. 5. Logic gate realization based on a single (top) and double (bottom) threshold mechanism.

In contrast to the typical nonlinearity with a single threshold, the nonlinearity used in this paper shows a special double-threshold behavior, i.e., the physical state undergoes an upward abrupt change when the input strength saturates, and undergoes another downward abrupt change when the input strength over saturates. The physical systems with such double-threshold behavior can not only realize the OR and AND gate, but also the XOR gate, as shown in the bottom panel of Fig. 5.

In this paper, the input is the polarization angle of the spin wave. The domain wall moves forward only if the polarization angle θ is close to 90° (or $|\sin\theta| \approx 1$), while the domain wall does not move when the polarization angle is much smaller or larger than 90° (e.g., $|\sin\theta| < 0.5$), thus realizing a double-threshold behavior as required.

Typically, the input strength is not easily tunable, and thus the threshold value needs to be adjusted to realize different gates, no matter it is for the single-threshold or double-threshold systems. Therefore, different gates would need different hard structures. However, for the magnetic logic in this paper, the threshold values remain unchanged, but the input strength (polarization angle here) can be easily modulated via tuning the initial polarization angle. Because of the double-threshold behavior and the polarization tunability, the magnetic logic gate is a universal logic gate, i.e., one hardware structure realizes all logic functionalities.

B. Nonvolatile computing

The spin-wave computing architecture proposed in this paper is of purely magnetic nature, where both the data storage and processing are achieved using magnetic elements. Since all inputs and outputs are stored in the nonvolatile racetrack memories, the magnetic logic naturally realizes nonvolatile memory-to-memory (or in-memory) computing. Because of this nature, the relatively short lifetime of spin wave is not a serious issue as long as it can sustain accomplishing one single operation, after which the result is stored. As a result, the hardware itself is not only programmable and can even evolve on real time, much more flexible than the field programmable gate arrays (FPGA). This capability makes it possible to realize evolvable hardware based on magnetic logic.

For a computing architecture to be fully functional and scalable, it has to meet the above five requirements: nonlinearity, Boolean functions, feedback elimination, gain and concatenability [39]. As for the present magnetic logic, the "nonlinearity" naturally comes from the double-threshold behavior of polarized-spin-wave-driven domain-wall motion in the logic track. Apparently, the magnetic logic here can realize all "Boolean functions", and in fact, using only one hard structure. "Feedback elimination" is ensured because the domain wall in logic track is constrained between P_1 and P_2 by gradient anisotropy, and thus its influence is not able to penetrate back into the input memory track. There is no "gain" issue neither, because the power is supplied through spin-wave injection in each logic track (via microwave through microantenna or spin current for instance), thus no gain from the input track is needed. And since both input and output of the logic are racetrack memories, the magnetic logic automatically possesses the "concatenability" by using the output track of one logic gate as the input track of the following logic gates.

VI. CONCLUSION

In conclusion, we introduce the concept of magnetic gating on spin-wave polarization, which gives rise to a purely magnetic analog of the Datta-Das spin transistor. Based on this magnetic gating effect, we propose a universal logic gate of purely magnetic nature, with data stored in the static magnetic textures (domains) and processed by its dynamical excitations (polarized spin wave). Because of its nonvolatility and universality, this magnetic logic concept provides new designing principles for in-memory processing.

ACKNOWLEDGMENTS

This work is supported by the National Natural Science Foundation of China (No. 11722430, No. 11847202). W.Y. is also supported by the China Postdoctoral Science Foundation (No. 2018M641906). J.L. is also supported by the China Postdoctoral Science Foundation (No. 2016M591594, No. 2017T100263), National Natural Science Foundation of China (No. 11904260), and the Startup Fund of Tianjin University. J.X. is also supported by the Shuguang Program of Shanghai Education Development Foundation and Shanghai Municipal Education Commission.

APPENDIX A: NUMERICAL METHOD

The functionalities of the proof-of-principle logic gates are verified via micromagnetic simulations. The simulations are performed in a two-dimensional environment built upon a self-developed Micromagnetic Module in COMSOL Multiphysics (a commercial software based on a finite-element method), where the LLG equation is transformed into weak form, and solved with a generalized alpha method [40–42]. Strict benchmarking is performed to ensure the correctness and robustness of this Micromagnetic Module. In comparison with the existing micromagnetic packages (such as MuMax or OOMMF), the advantage of this COMSOL-based Micromagnetic Module lies in that it can easily deal with complicated device structures such as the ones studied in this paper. The same method has been applied in several cases, including both ferromagnetic and antiferromagnetic systems [20,22,29,43].

The magnetization dynamics of the SyAF structure is described by the coupled LLG equations for each sublayer [22,44],

$$\dot{\mathbf{m}}_j(r,t) = -\gamma \mathbf{m}_j(r,t) \times \mathbf{H}_j^{\text{eff}} + \alpha_j \mathbf{m}_j(r,t) \times \dot{\mathbf{m}}_j(r,t) + \boldsymbol{\tau}_j, \tag{A1}$$

where $j = 1, 2, 3$ denotes the lower and upper layer of the logic track and the memory track above, respectively. Here $\gamma = 2.21 \times 10^5$ Hz m/A is the gyromagnetic ratio, α_j is the Gilbert damping constant for the jth layer.

$$\mathbf{H}_j^{\text{eff}} = K m_j^z \hat{\mathbf{z}} + A\nabla^2 \mathbf{m}_j + D\left[\left(\nabla \cdot \mathbf{m}_j\right)\hat{\mathbf{z}} - \nabla m_j^z\right] - J\mathbf{m}_{\bar{j}} \tag{A2}$$

is the effective field acting locally on sublayer $\mathbf{m}_j$, with $\bar{j}$ denoting the neighbouring layer of jth layer. The parameters are taken as the following: the perpendicular easy-axis anisotropy $K = 3.88 \times 10^4$ A/m, the exchange coupling constant $A = 3.28 \times 10^{-11}$ A m, the coefficient of interfacial DMI $D = 1.4 \times 10^{-3}$ A [22], and the antiferromagnetic exchange coupling due to RKKY interaction in the logic track is $J = 1.0 \times 10^6$ A/m. These values all fall into the reasonable range of conventional SyAF structures [31]. The effects of the dipolar fields are neglected in micromagnetic simulations because of two reasons: (i) the static dipolar field effectively only reduces the anisotropy K and the interlayer coupling J' (see Supplemental Material) [45], (ii) the spin waves used are exchange spin wave with very short wavelength for which the long-range dynamical dipolar interaction can be ignored. Clocked current pulses (interval 10 ns, duration 0.8 ns) are applied in the memory track to shift the memory bit in the racetrack. The current-induced spin transfer torque in the memory track is taken as $\boldsymbol{\tau}_3 = (\mathbf{u}\cdot\nabla)\mathbf{m}_3 - \beta\mathbf{m}_3 \times (\mathbf{u}\cdot\nabla)\mathbf{m}_3$ [46,47], where $\mathbf{u} = u_0\hat{\mathbf{y}}$ with $u_0 = \pm 500$ m/s represents the current flowing in certain direction $\hat{\mathbf{y}}$ (in $\mp y$ direction for the current in input and output track in Fig. 2). The Gilbert damping $\alpha_{1,2}$ in the logic track is taken as 4×10^{-4}, for which the spin wave can propagate up to 10 μm, sufficient for the purpose of logical operation considered in this paper. The damping constant is set to $\alpha_3 = 0.2$ [48] in the memory track to guarantee the stability of current-driven domain-wall motion, and the nonadiabatic coefficient is $\beta = 0.2$. The exact value of β is not crucial in this work.

APPENDIX B: MODELING OF THE MAGNETIC LOGIC GATE

The width of the logic track is 200 nm, and the width of the memory track is $l = 240$ nm. In this trilayer retarder structure, the antiferromagnetic exchange coupling between the memory track and the logic track is $2J' = 1.35 \times 10^4$ A/m.

In the writing region, an asymmetric coupling between the logic track and the memory track is built in, i.e., magnetization in the logic track can be easily imprinted into the memory track, while magnetization in the memory track has little effect on the magnetization in the logic track. Such an effect can be realized by various approaches. One way is to make the total magnetization of the output memory track at the crossing section much smaller than that of the logic track, which can be realized by either reducing the memory-track thickness or using softer magnetic materials in the memory track.

The domain wall in the logic track has two stable positions: P_1 and P_2. P_1 is its natural position in the absence of driving forces (from injected spin wave), and P_2 is the position when there is sufficient driving force. Such domain-wall motion behavior is realized by building in an anisotropy gradient between P_1 and P_2 in the logic track. P_1 is the location with the minimum magnetic anisotropy. And the slope of the gradient defines the minimum force required for the domain wall being pushed to P_2. Such an anisotropy gradient can be realized experimentally by various means, e.g., by ion irradiation [37] or geometric thickness and width modulation [49,50]. In our simulation, the anisotropy gradient is taken as 2×10^9 A/m^2. When the driving force due to the reflected spin wave overcomes the anisotropy gradient, the domain wall moves away against the gradient. Due to the attenuation of spin waves, the competition between the spin-wave driving force and the anisotropy gradient reaches balance, and the domain wall is finally stabilized at P_2. In the simulations, we set a high-damping region around P_2 to attenuate the spin waves (which can be easily realized in experiments by covering a metal stripe). When the driving force exerted by the spin waves is not strong enough, the domain wall will naturally come back to P_1. The duration between two sequent operation is chosen as 10 ns (corresponding to clocking rate 0.1 GHz), which is long enough for the domain wall to reach its stable position, so that the logic gate is reliable and can work correctly for sequent operations. The stability has been demonstrated by the micromagnetic simulation (see Videos 1–3).

[1] Mark Lundstrom, Moore's law forever?, Science **299**, 210 (2003).

[2] T. N. Theis and H. S. P. Wong, *The End of Moore's Law: A New Beginning for Information Technology* (IEEE Educational Activities Department, 2017), Vol. 19, p. 41.

[3] Igor L. Markov, Limits on fundamental limits to computation, Nature **512**, 147 (2014).

[4] M. N. Baibich, J. M. Broto, A. Fert, F. Nguyen Van Dau, F. Petroff, P. Etienne, G. Creuzet, A. Friederich, and J. Chazelas, Giant Magnetoresistance of (001)Fe/(001)Cr Magnetic Superlattices, Phys. Rev. Lett. **61**, 2472 (1988).

[5] G. Binasch, P. Grünberg, F. Saurenbach, and W. Zinn, Enhanced magnetoresistance in layered magnetic structures with antiferromagnetic interlayer exchange, Phys. Rev. B **39**, 4828 (1989).

[6] J. C. Slonczewski, Current-driven excitation of magnetic multilayers, J. Magn. Magn. Mater. **159**, L1 (1996).

[7] L. Berger, Emission of spin waves by a magnetic multilayer traversed by a current, Phys. Rev. B **54**, 9353 (1996).

[8] A. Manchon, J. Zelezny, I. M. Miron, T. Jungwirth, J. Sinova, A. Thiaville, K. Garello, and P. Gambardella, Current-induced spin-orbit torques in ferromagnetic and antiferromagnetic systems, Rev. Mod. Phys. **91**, 035004 (2019).

[9] Stuart S. P. Parkin, Masamitsu Hayashi, and Luc Thomas, Magnetic domain-wall racetrack memory, Science **320**, 190 (2008).

[10] Stuart Parkin and See-Hun Yang, Memory on the racetrack, Nat. Nanotech. **10**, 195 (2015).

[11] Y. Kajiwara, K. Harii, S. Takahashi, J. Ohe, K. Uchida, M. Mizuguchi, H. Umezawa, H. Kawai, K. Ando, K. Takanashi, S. Maekawa, and E. Saitoh, Transmission of electrical signals by spin-wave interconversion in a magnetic insulator, Nature **464**, 262 (2010).

[12] A. V. Chumak, V. I. Vasyuchka, A. A. Serga, and B. Hillebrands, Magnon spintronics, Nat. Phys. **11**, 453 (2015).

[13] Jiahao Han, Pengxiang Zhang, Justin T. Hou, Saima A. Siddiqui, and Luqiao Liu, Mutual control of coherent spin waves and magnetic domain walls in a magnonic device, Science **366**, 1121 (2019).

[14] Alexander Khitun and Kang L. Wang, Nano scale computational architectures with spin wave bus, Superlattice Microst. **38**, 184 (2005).

[15] Alexander Khitun, Mingqiang Bao, and Kang L. Wang, Magnonic logic circuits, J. Phys. D: Appl. Phys. **43**, 264005 (2010).

[16] T. Schneider, A. A. Serga, B. Leven, B. Hillebrands, R. L. Stamps, and M. P. Kostylev, Realization of spin-wave logic gates, Appl. Phys. Lett. **92**, 022505 (2008).

[17] Vladimir L. Safonov, *Nonequilibrium Magnons: Theory, Experiment and Applications* (John Wiley & Sons, Weinheim, Germany, 2012).

[18] K. Vogt, F. Y. Fradin, J. E. Pearson, T. Sebastian, S. D. Bader, B. Hillebrands, A. Hoffmann, and H. Schultheiss, Realization of a spin-wave multiplexer, Nat. Commun. **5**, 3727 (2014).

[19] Andrii V. Chumak, Alexander A. Serga, and Burkard Hillebrands, Magnon transistor for all-magnon data processing, Nat. Commun. **5**, 4700 (2014).

[20] Jin Lan, Weichao Yu, Ruqian Wu, and Jiang Xiao, Spin-Wave Diode, Phys. Rev. X **5**, 041049 (2015).

[21] S. Klingler, P. Pirro, T. Bracher, B. Leven, B. Hillebrands, and A. V. Chumak, Spin-wave logic devices based on isotropic forward volume magnetostatic waves, Appl. Phys. Lett. **106**, 212406 (2015).

[22] Jin Lan, Weichao Yu, and Jiang Xiao, Antiferromagnetic domain wall as spin wave polarizer and retarder, Nat. Commun. **8**, 178 (2017).

[23] F. Keffer and C. Kittel, Theory of antiferromagnetic resonance, Phys. Rev. **85**, 329 (1952).

[24] Ran Cheng, Matthew W. Daniels, Jian-Gang Zhu, and Di Xiao, Antiferromagnetic spin wave field-effect transistor, Sci. Rep. **6**, 24223 (2016).

[25] G. Gitgeatpong, Y. Zhao, P. Piyawongwatthana, Y. Qiu, L. W. Harriger, N. P. Butch, T. J. Sato, and K. Matan, Nonreciprocal Magnons and Symmetry-Breaking in the Noncentrosymmetric Antiferromagnet, Phys. Rev. Lett. **119**, 047201 (2017).

[26] Igor Proskurin, Robert L. Stamps, Alexander S. Ovchinnikov, and Jun-ichiro Kishine, Spin-Wave Chirality and its Manifestations in Antiferromagnets, Phys. Rev. Lett. **119**, 177202 (2017).

[27] Alireza Qaiumzadeh, Lars A. Kristiansen, and Arne Brataas, Controlling chiral domain walls in antiferromagnets using spin-wave helicity, Phys. Rev. B **97**, 020402 (2018).

[28] Matthew W. Daniels, Ran Cheng, Weichao Yu, Jiang Xiao, and Di Xiao, Nonabelian magnonics in antiferromagnets, Phys. Rev. B **98**, 134450 (2018).

[29] Weichao Yu, Jin Lan, and Jiang Xiao, Polarization-selective spin wave driven domain-wall motion in antiferromagnets, Phys. Rev. B **98**, 144422 (2018).

[30] See-Hun Yang, Kwang-Su Ryu, and Stuart Parkin, Domain-wall velocities of up to 750 ms^{-1} driven by exchange-coupling torque in synthetic antiferromagnets, Nat. Nanotech. **10**, 221 (2015).

[31] R. A. Duine, Kyung-Jin Lee, Stuart S. P. Parkin, and M. D. Stiles, Synthetic antiferromagnetic spintronics, Nat. Phys. **14**, 217 (2018).

[32] S. S. P. Parkin, N. More, and K. P. Roche, Oscillations in Exchange Coupling and Magnetoresistance in Metallic Superlattice Structures: Co/Ru, Co/Cr, and Fe/Cr, Phys. Rev. Lett. **64**, 2304 (1990).

[33] A. G. Gurevich and G. A. Melkov, Magnetization Oscillations and Waves (CRC Press, Boca Raton, Florida, 1996).

[34] R. I. Joseph and E. Schlömann, Demagnetizing field in nonellipsoidal bodies, J. Appl. Phys. **36**, 1579 (1965).

[35] J. Nogués and Ivan K. Schuller, Exchange bias, J. Magn. Magn. Mater. **192**, 203 (1999).

[36] Supriyo Datta and Biswajit Das, Electronic analog of the electro-optic modulator, Appl. Phys. Lett. **56**, 665 (1990).

[37] J. H. Franken, H. J. M. Swagten, and B. Koopmans, Shift registers based on magnetic domain wall ratchets with perpendicular anisotropy, Nat. Nanotech. **7**, 499 (2012).

[38] The rotation angle is reduced because of partial reflection of $\hat{\mathbf{x}}$ polarization at $f = 11$ GHz.

[39] Behtash Behin-Aein, Deepanjan Datta, Sayeef Salahuddin, and Supriyo Datta, Proposal for an all-spin logic device with built-in memory, Nat. Nanotech. **5**, 266 (2010).

[40] Helga Szambolics, L. Buda-Prejbeanu, J. Toussaint, and Olivier Fruchart, in *Proceedings of the COMSOL Users Conference* (COMSOL AB, Stockholm, Sweden, 2006).

[41] François Alouges, Evaggelos Kritsikis, and Jean-Christophe Toussaint, A convergent finite element approximation for Landau-Lifschitz-Gilbert equation, Physica B: Condensed Matter 8th International Symposium on Hysteresis Modeling and Micromagnetics (HMM 2011) 407, 1345 (2012).

[42] COMSOL Multiphysics® v. 5.4. www.comsol.com. COMSOL AB, Stockholm, Sweden.

[43] Weichao Yu, Jin Lan, Ruqian Wu, and Jiang Xiao, Magnetic Snell's law and spin-wave fiber with Dzyaloshinskii-Moriya interaction, Phys. Rev. B **94**, 140410 (2016).
[44] Ran Cheng, Jiang Xiao, Qian Niu, and Arne Brataas, Spin Pumping and Spin-Transfer Torques in Antiferromagnets, Phys. Rev. Lett. **113**, 057601 (2014).
[45] See Supplemental Material http://link.aps.org/supplemental/10.1103/PhysRevApplied.13.024055 on the influence of the dipolar field.
[46] Z. Li and S. Zhang, Domain-Wall Dynamics and Spin-Wave Excitations with Spin-Transfer Torques, Phys. Rev. Lett. **92**, 207203 (2004).
[47] Soo-Man Seo, Kyung-Jin Lee, Hyunsoo Yang, and Teruo Ono, Current-Induced Control of Spin-Wave Attenuation, Phys. Rev. Lett. **102**, 147202 (2009).
[48] Yan Zhou and Motohiko Ezawa, A reversible conversion between a skyrmion and a domain-wall pair in a junction geometry, Nat. Commun. **5**, 4652 (2014).
[49] Sai Li, Wang Kang, Yangqi Huang, Xichao Zhang, Yan Zhou, and Weisheng Zhao, Magnetic skyrmion-based artificial neuron device, Nanotechnology **28**, 31LT01 (2017).
[50] Xing Chen, Wang Kang, Daoqian Zhu, Xichao Zhang, Na Lei, Youguang Zhang, Yan Zhou, and Weisheng Zhao, A compact skyrmionic leaky-integrate-fire spiking neuron device, Nanoscale **10**, 6139 (2018).